

17. R. Shiller, *ibid.*, p. 499.
18. J. Campbell and R. Shiller, unpublished manuscript.
19. S. Grossman, A. Melino, R. Shiller, "Estimating the continuous time consumption based asset pricing model" (Working paper 1643, National Bureau of Economic Research, Cambridge, MA, 1985).
20. R. Shiller, *Carnegie Rochester Conf. Ser. Public Policy* 17, 203 (1982).
21. B. Mandelbrot, *J. Bus.* 36, 394 (1963).
22. T. Bollerslev, "A conditionally heteroskedastic time series model for security prices and rates of return data" (discussion paper 85-32, Department of Economics, University of California, San Diego, 1985).
23. L. Summers, *J. Financ.* 41, 591 (1986).
24. Alfred Cowles & Associates, *Common Stock Indexes* (Principia, Bloomington, IN, ed. 2, 1939).
25. Supported by NSF grant SES-8520075.

Laser Remote Sensing of the Atmosphere

DENNIS K. KILLINGER AND NORMAN MENYUK

Laser beams can be used as long-range spectroscopic probes of the chemical composition and physical state of the atmosphere. The spectroscopic, optical, and laser requirements for atmospheric laser remote sensing are reviewed, and the sensitivity and limitations of the technique are described. A sampling of recent measurements includes the detection of urban air pollution and toxic chemicals in the atmosphere, the measurement of global circulation of volcanic ash in the upper atmosphere, and the observation of wind shear near airports.

LASER REMOTE SENSING OF ATMOSPHERIC PROPERTIES from a single location is referred to as lidar, an acronym for light detection and ranging, and is analogous to radar (1-6). In lidar, the projection of a short laser pulse is followed by reception of a portion of the radiation reflected from a distant target or from atmospheric constituents such as molecules, aerosols, clouds, or dust (Fig. 1). The incident laser radiation interacts with these constituents, causing alterations in the intensity and wavelength according to the strength of this optical interaction and the concentration of the interacting species in the atmosphere. Consequently, information on the composition and physical state of the atmosphere can be deduced from the lidar data. In addition, the range to the interacting species can be determined from the temporal delay of the backscattered radiation. Lidar has been used to measure the movement and concentration of air pollution near urban centers, the chemical emission around industrial plants, and atmospheric trace chemicals in the stratosphere. Lidar has also been used to measure the velocity and direction of winds near storms and airports and to track the global circulation of volcanic ash emitted into the atmosphere after recent eruptions, such as those at Mount St. Helens and El Chichón. Under optimal conditions lidar can be extremely sensitive. An example is the ground-based laser remote sensing of sodium and lithium atoms in the stratosphere at ranges greater than 90 km and in concentrations as low as a few atoms per cubic centimeter (5). More commonly, detection ranges are on the order of a few hundred meters to several kilometers and concentration levels on the order of parts per million to parts per billion.

The use of optical backscatter to measure properties of the atmosphere is not new, extensive experiments having been conducted in the early 1900's with large searchlights. The field of optical

remote sensing was greatly advanced by the laser, which offers several improvements over conventional light sources. These include narrow spectral width (<0.01 nm), a frequency or color that is often tunable, and high peak power ($>10^6$ W) available in a short pulse (<1 μ sec) and in a narrow beam (<10 cm in diameter). These attributes make the laser an ideal spectroscopic probe of the atmosphere. In this regard, a lidar system may be thought of as an "active" remote sensing system since it can illuminate the target region, in contrast to a "passive" optical sensor which detects ambient light or thermal emission from the target.

The applications of lidar systems for the remote sensing of atmospheric properties were appreciated soon after the discovery of lasers in the early 1960's. Early lidar measurements were made in 1962 by Fiocco and Smullin (7) who bounced a laser beam off the moon and who also investigated the turbid layers in the upper atmosphere; in 1963 by Ligda (8) who used a ruby laser to obtain the first lidar measurements of cloud heights and tropospheric aerosols; and in 1964 by Schotland (9) who used a temperature-tuned ruby laser to detect water vapor in the atmosphere. Progress has been continuous since that time, but the discovery of different laser sources in the past decade, coupled to improvements in optical instrumentation and data processing, has been responsible for the recent surge in the number of laser remote sensing systems. This improved capability has been accompanied by an increased awareness of the need to monitor the impact of natural and anthropogenic influences on the environment.

Remote sensing of the atmosphere by optical techniques can be accomplished in several ways. One technique involves measurement of the absorption spectrum of the atmosphere over a long path separating a spectroscopic optical source and a detector (5). Another long-path absorption technique uses a configuration, described by Hinkley and Kelley (10), in which a tunable laser source and detector are located together and a retroreflecting mirror is placed at a distance of several hundred meters; such a system is useful when the laser source is weak, since the retroreflector greatly enhances the returned radiation. In this article we will primarily be concerned with a pulsed lidar system where the laser and detector are located together and no retroreflector is used as the target; in this case the returned laser radiation is due to backscatter from aerosols or dust in the atmosphere or a topographic target such as a hill or trees.

The authors are at the Massachusetts Institute of Technology, Lincoln Laboratory, Lexington, MA 02173-0073.

Optical Requirements for Laser Remote Sensing

The physics and optical technology associated with atmospheric laser remote sensing encompass atmospheric optical propagation, atomic and molecular spectroscopy, digital signal processing, and laser technology. In this section we discuss the optical requirements for lidar and, in particular, review (i) the presence of transmission "windows" in the atmosphere which permit the laser beam to propagate through the atmosphere with little attenuation, (ii) the identification and relative strength of the various optical interactions between an atmospheric species and a laser beam, and (iii) the properties of suitable lasers.

Atmospheric transmission windows. For a laser beam to detect a species at a long distance, the beam must not be appreciably attenuated by the intervening atmosphere. The output wavelength of the laser must therefore lie in a spectral transmission "window" of the atmosphere. These windows are shown as clear areas in Fig. 2, which shows a low-resolution transmission spectrum of the atmosphere over the spectral region from the ultraviolet to the mid-infrared (15 μm) for a path of 300 m (11). The atmosphere has regions of strong absorption as well as transmission windows; the absorption regions are due primarily to oxygen, carbon dioxide, and water vapor, and exhibit finer detail than that shown in the figure. The most useful transparent spectral ranges of the atmosphere are the visible (0.4 to 0.7 μm), near infrared (0.7 to 1.5 μm), and 3- to 5- μm and 9- to 13- μm regions. Within these spectral regions, the laser is not appreciably attenuated except by clouds, and thus remote sensing over long distances may be achieved.

Optical interaction of lasers with atmospheric species. The primary influence of the atmosphere on a low-power laser beam is through scattering and absorption. Both processes cause an attenuation of the beam according to Bouguer's or Beer's law

$$I = I_0 e^{-\alpha R} \quad (1)$$

where I is the intensity of the optical beam after transmission over a distance R , α is the atmospheric extinction coefficient, and I_0 is the initial intensity of the beam. It is possible to express α as a sum of terms

$$\alpha = \alpha_{\text{Ray}} + \alpha_{\text{Mie}} + \alpha_{\text{Raman}} + \alpha_{\text{abs}} \quad (2)$$

where α_{Ray} , α_{Mie} , and α_{Raman} are the extinction coefficients related to Rayleigh, Mie, and Raman scattering, respectively, and α_{abs} is the molecular absorption coefficient (3). Rayleigh scattering is due to particles in the atmosphere, such as molecules or fine dust, that are much smaller than the optical wavelength, λ , of the laser. Mie scattering is associated with larger particles such as aerosols whose size is on the order of λ . Rayleigh and Mie processes are elastic scattering: the scattered light is the same wavelength (color) as the incident laser beam. Raman scattering is an inelastic interaction of the optical beam involving excitation of the energy levels of a molecule and reradiation at a different wavelength. Absorption of the laser beam is a resonant interaction (direct absorption) leading to excitation of the molecule, followed possibly by fluorescence.

The sensitivity of laser remote sensing is related to the relative strength of these optical processes through the "lidar equation." The lidar equation (2, 3) is used to predict the power of the backscattered signal, P_r , and may be given in the form

$$P_r = \frac{P_t \rho A K e^{-2\alpha R}}{\pi R^2} \quad (3)$$

where P_t is the transmitted laser power, R is the range to the target, ρ is the effective reflectivity of the target (assumed to be larger than the laser beam), which backscatters the radiation into π steradians,

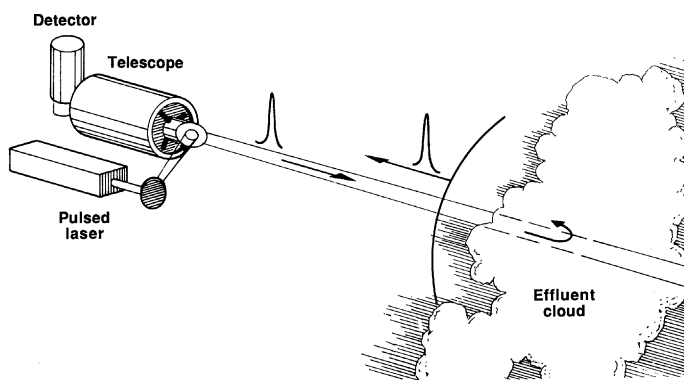


Fig. 1. Schematic of a lidar used for laser remote sensing of the atmosphere. The backscattered laser radiation may contain spectral information on the composition and physical condition of the cloud or the intervening atmosphere.

A is the area of the telescope, K is the optical efficiency of the system, and $\exp(-2\alpha R)$ is the two-way atmospheric attenuation of the optical beam. The more general form of Eq. 3 contains integrals over range, time, and spectral wavelength (6). The target can be either a solid reflector, such as a building or trees, or a "distributed" reflector consisting of molecules, dust, or clouds in the atmosphere. In the latter case, the target reflectivity term, ρ , is due to Mie, Rayleigh, Raman, or fluorescence processes and is thus also related to the associated α values.

The approximate strength of these processes is given in Table 1, which lists typical maximum values of ρ and α for some of the most important optical interactions (3, 6). The contribution of the scattering processes to both α and ρ arises because scattering reduces the intensity of the laser beam, contributing to extinction, whereas the portion of the beam that is scattered by 180° contributes to the detected signal, thereby serving effectively as a reflector. Absorption contributes only to the extinction coefficient, with no intrinsic contribution to ρ . In Table 1, values are given for ρ in conjunction with absorption, and refer to effective reflectivities arising from

Table 1. Optical interactions for laser remote sensing of the atmosphere; N.A., not applicable.

Optical interaction	Spectral range (μm)	Scatterer	Attenuation* α (km^{-1})	Effective† reflectivity ρ	
Absorption (resonant)	UV	Atoms, molecules	10^7	10^{-2}	
	1		10^6	10^{-3} to 10^{-1}	
	10		10^5	10^{-7} to 10^{-4}	
Scattering (non-resonant)	Rayleigh	O_2, N_2	10^{-1}	10^{-3}	
			1	10^{-3}	10^{-5}
			10	10^{-7}	10^{-9}
	Mie	Aerosols, fine dust	10^{-1}	10^{-3}	
			1	10^{-1}	10^{-4}
	10	10^{-2}	10^{-5}		
Raman	UV	Molecules	10^{-5}	10^{-7}	
			1	10^{-7}	10^{-9}
			10	10^{-11}	10^{-13}
Backscatter by hard targets	UV-IR	Buildings, trees, dense clouds	N.A.	10^{-2} to 1	

*Attenuation calculated for concentration of 1 atm. †Reflectivity calculated for range resolution of 100 m, 1 atm concentration, and isotropic scattering.

fluorescence emission of the atom or molecule after it has absorbed the incident light (12). Conversely, a topographic target does not contribute to signal extinction; instead, the 180° scattered portion of the incident beam corresponds to the effective target reflectivity.

In general, the value of ρ or α may be a complicated function of laser linewidth, wavelength, or spectral filtering in the detection process, and may exhibit strong resonances. The values presented in Table 1 are appropriate to the strong resonance case and are appropriate only if the laser spectral requirements are met. The large values for α shown for absorption are for the case where the laser wavelength is coincident with an absorption line of the molecule; off-resonant values of α are orders of magnitude smaller. The backscatter and absorption coefficients, in general, depend on species concentration, temperature, pressure, and possibly velocity, so that lidar can measure one or more of these parameters. Measurements for all lidar systems are based on changes in the returned signal, P_r , as a function of wavelength or range, and thus deduce information about the physical state of the atmosphere through the effect of α or ρ .

A wide range of values occur for α and ρ (Table 1). Since all optical processes shown can occur simultaneously, it is important to design the lidar system, through judicious choice of laser wavelength, spectral filtering, or geometry, so that the measurement is most sensitive to only one optical interaction. In some lidar designs, α and ρ depend on different optical interactions; in other words, the attenuation and backscatter arise from different processes.

Lidar systems that measure a particular optical interaction have been classified as follows: (i) atmospheric backscatter lidar, (ii) differential-absorption lidar (DIAL), (iii) fluorescence lidar, (iv) Raman lidar, and (v) Doppler lidar. These classifications refer to the optical interaction to which the system has been designed to be most sensitive. Atmospheric backscatter lidar transmits one laser wavelength and detects changes in the backscatter due to the aerosols or dust in the atmosphere. DIAL measures the concentration of a molecular species in the atmosphere by transmitting two wavelengths, only one of which is absorbed, and detecting the difference in the intensity of the returns at the two wavelengths; the backscatter in DIAL may be from a hard target, or aerosol and dust returns as in atmospheric backscatter lidar. Fluorescence lidar uses two wavelengths as in a DIAL system and in addition uses spectrometric techniques to separate the wavelength-shifted fluorescence signal from the strong Rayleigh backscatter in the atmosphere. Raman and Doppler lidar uses a single-wavelength laser and sophisticated spectrometric detection techniques to spectrally resolve the wavelength-shifted signal from the strong background due to Rayleigh or Mie scattering. A Raman measurement often detects a wide spectral range (~ 10 nm) containing a number of vibrational-rotational Raman-shifted lines, whereas a Doppler measurement detects only a very narrow spectral range ($\sim 10^{-5}$ nm) that encompasses the Doppler-shifted backscatter lidar return. Because DIAL, fluorescence, and Raman techniques use several wavelengths that are either transmitted by the laser or detected by the lidar system, they provide measurements of the absolute concentration of the detected species. In contrast, atmospheric backscatter lidar uses a single-wavelength laser and single-wavelength detection and is best suited for lidar measurements that determine relative changes in the density of a known atmospheric species; these relative density measurements may, however, be referenced to an absolute value if the lidar is calibrated with the use of a standard target.

Laser sources. The utility of laser remote sensing is dependent on several factors, including the availability of lasers with sufficient output power and wavelength characteristics to provide an adequate lidar signal. Although many lasers provide high power, they often

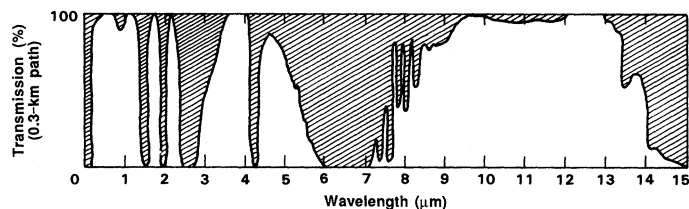


Fig. 2. Optical transmission of the atmosphere depicting the presence of strong absorption bands and transmission "windows" in the atmosphere.

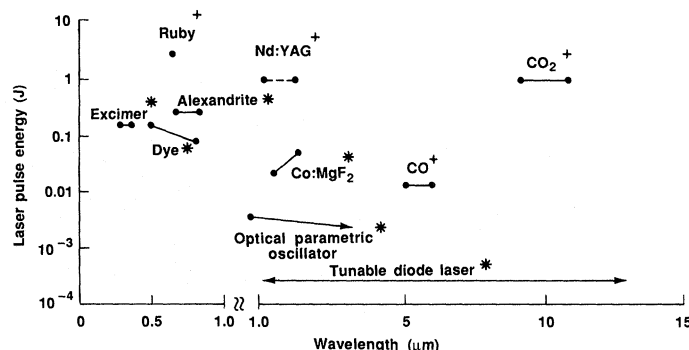


Fig. 3. Typical values of laser pulse energy as a function of laser wavelength tuning range showing the gaps in wavelength coverage of currently available lasers; (+) line tunable; (*) continuously tunable.

lack spectral coverage or tunability, preventing a determination of the resonant values of α or ρ (Table 1) for the particular atmospheric species or for the optical parameter of interest.

This may be better understood on the basis of Fig. 3, which presents the output energy per pulse now available from commercially available pulsed lasers of moderate size as a function of their wavelength coverage (13, 14). The wavelength tuning range of high-power lasers is not complete across the spectral range shown and is particularly lacking in the "eye-safe" spectral region ($\lambda > 1.4$ μm). For remote sensing in the infrared (IR), a minimum transmitted laser pulse energy on the order of 1 to 10 mJ is required for the detection of lidar signals from a hard target at a range of a few kilometers, and about 1 J for range-resolved returns from atmospheric aerosols. These values may be lowered by one to two orders of magnitude if heterodyne detection can be used to detect the IR lidar return or if the remote sensing can be conducted in the visible or ultraviolet (UV). The detection of lidar atmospheric backscatter is much more sensitive in the latter spectral regions because detectors less susceptible to noise (such as photomultiplier tubes) are available and the atmospheric backscatter is improved in the UV-visible as compared to the IR.

The characteristics shown in Fig. 3 demonstrate why most laser remote sensing experiments have used ruby, dye, neodymium:yttrium-aluminum-garnet (Nd:YAG), and CO₂ lasers. These lasers offer sufficient energy for the detection of atmospheric species at moderate ranges, operate at wavelengths that are not appreciably attenuated by the atmosphere, and occur in a spectral range where several atmospheric constituents have reasonably strong optical interactions. Some of the lasers shown, such as Nd:YAG, CO, and CO₂, are line tunable in that they operate only on a limited number of discrete lines or wavelengths. The other lasers are continuously tunable within the spectral range shown in Fig. 3. Single-wavelength lasers are suitable for atmospheric backscatter, Raman, and Doppler lidar measurements since the spectral information is obtained during the detection process with a spectrometer or spectral filter. Lasers for DIAL or fluorescence lidar must be tunable, however, so that the laser wavelength can match the resonance

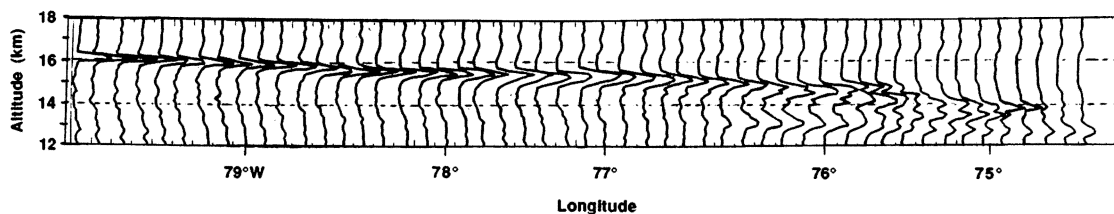


Fig. 4. Airborne lidar returns as a function of altitude and longitude near the coast of South Carolina on the evening of 27 May 1980 showing the increased lidar backscatter in a layer near 14 to 16 km due to volcanic material injected into the atmosphere by Mount St. Helens volcano. [Adapted from (16)]

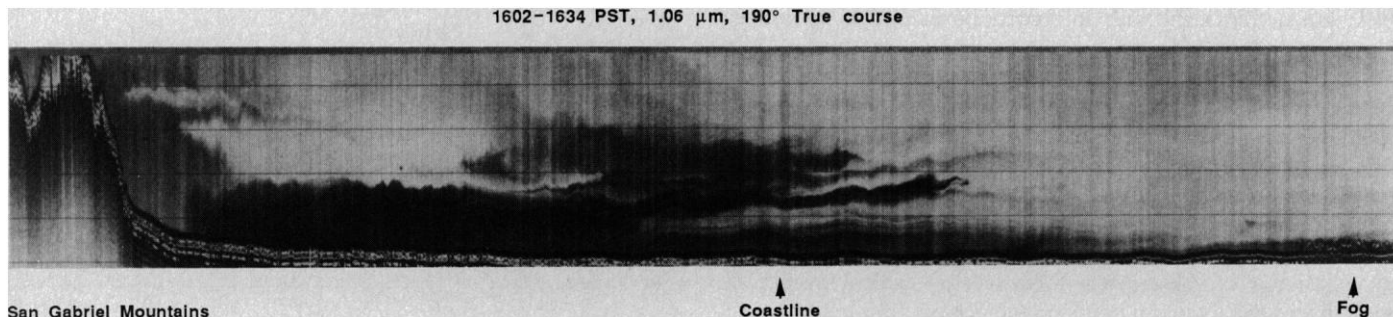


Fig. 5. Airborne lidar data near Los Angeles showing the vertical density profile of the boundary layer and continental flow of urban haze. [Adapted from (17)]

wavelength of the optical absorption lines of the molecules or atoms being detected. This is most important for the remote sensing of molecules or pollutants in the atmosphere because most of the absorption lines of many important organic species occur in the middle IR (2 to 5 μm) and this “fingerprint” spectral region does not coincide with many high-power, tunable laser sources. Because of these considerations, one of the most important goals in the future application of laser remote sensing is the development of new, high-power tunable lasers to cover the spectral gaps shown in Fig. 3.

Lidar Atmospheric Measurements

Each of the five lidar types can be used for the remote sensing of a selected variety of atmospheric constituents or parameters. Table 2 lists some of the constituents and parameters that have been measured with lidar. More detail is available in the technical digests of several recent lidar conferences (15).

Atmospheric backscatter lidar. Atmospheric backscatter lidar is the most common type of lidar system and consists of a nontunable, high-power, pulsed laser that is used to measure changes in the density or backscatter coefficient of the atmosphere that are due to particulates, such as aerosols, clouds, dust, or plumes. These atmospheric constituents have relatively large optical scattering cross sections and are relatively easy to detect (Table 1). Such lidars have been useful in tracking the turbid effluent and gas plumes from industrial smokestacks and have also been used to map out rain, snow, ice crystals, and dense clouds in the atmosphere (1). Precision measurements of the slight changes in the vertical density of the atmosphere have also been made with lidar, from which one can determine the pressure and temperature of the atmosphere as a function of altitude (15).

Recently, McCormick used a lidar system to track and map out the density of volcanic ash emitted into the atmosphere by Mount St. Helens and El Chichón (16). Figure 4 presents data obtained by McCormick using an airborne lidar system incorporating a high-power, frequency-doubled Nd:YAG laser operating near 0.53 μm (16). A thick layer of volcanic ash was detected at an altitude near 16

km and was found to vary in density and stratification as a function of distance. By tracking the cloud of volcanic ash, McCormick was able to use the ash as a tracer for global wind and circulation patterns. Such data, coupled with IR satellite data, showed the kinetics of global atmospheric circulation and tracked the slow global mixing of the volcanic ash between the Northern Hemisphere and the Southern Hemisphere that occurred the following year.

Atmospheric aerosols have also been studied by lidar in both the troposphere and the stratosphere. Lidar systems with beam-steering capabilities have been used by Uthe *et al.* for three-dimensional mapping of the flow of dense tropospheric aerosols (haze) near the ocean-land boundary and urban centers (17). An example of such measurements obtained near Los Angeles, showing the flow patterns of urban aerosols, is given in Fig. 5 (17). Such data have greatly increased our knowledge of the interplay of air circulation and pollution emission and are being used to predict the impact of emissions near urban centers.

Atmospheric backscatter lidar has been instrumental in investigations of the propagation of a laser beam through the atmosphere. These investigations have included the study of complicated scattering processes (1) present under normal atmospheric conditions due to the statistical distribution and variability of aerosols and scattering particles (18). In addition, the effect of multiple scattering has been investigated by lidar; multiple scattering is due to optically thick clouds that can drastically alter the transmission properties of a laser beam from that described by Eq. 1 (19).

Differential-absorption lidar. Most lidar measurements that determine the concentration of gaseous species in the atmosphere are presently made with the DIAL technique (20). This technique uses two or more wavelengths to measure the difference in the absorption of the lidar signal as the laser frequency is varied between a wavelength that is absorbed by molecules in the atmosphere and a wavelength that is not absorbed. The method is sensitive because it takes advantage of the relatively large value of the “on-resonance” absorption coefficient α (Table 1).

In principle, the concentration of an atmospheric species may be obtained directly from Eqs. 2 and 3 on the basis of measurements at a single wavelength. However, a concentration determination based on Eq. 3 and a single-wavelength measurement requires an accurate

knowledge of K , ρ , α , and the geometric factors R and A . In general, these parameters are either unknown or known with poor accuracy.

The DIAL technique attempts to overcome this problem by measuring the lidar signals at two wavelengths, λ and λ' . The laser wavelength λ is chosen to coincide with a wavelength strongly absorbed by the molecule being investigated, while at λ' there is little or no absorption. The use of two wavelengths results in two equations of the form of Eq. 3, which are then solved simultaneously for N_a , the path-averaged concentration of the absorbing molecule to yield

$$N_a = \frac{1}{2(\sigma_a' - \sigma_a)R} \left[\ln\left(\frac{P}{P'}\right) + \ln\left(\frac{\rho'}{\rho}\right) + 2(\alpha - \alpha')R \right] \quad (4)$$

where σ_a is the absorption cross section of the absorbing molecule, P is the backscattered signal power normalized to the transmitted power ($P = P_r/P_t$), and the primed and unprimed parameters refer to values at the low- and high-absorption wavelengths λ' and λ , respectively (20). In deriving Eq. 4 from Eq. 3, the $e^{-2\alpha R}$ term in Eq. 3 has been replaced by $e^{-2(\alpha + N_a\sigma_a)R}$, where α now represents the assumed known total attenuation of the atmosphere except that due to absorption, and $N_a\sigma_a$ is the attenuation due to absorption by the molecule being investigated.

The advantage of this two-frequency (DIAL) approach is that only differences in the various parameters need be considered. For this reason the DIAL technique is more commonly used for species concentration determination than single-frequency absorption measurements, despite the added complexity of a dual-frequency lidar system. Further simplification can be achieved when the use of closely spaced frequencies in a given measurement results in differences of target reflectivity ($\Delta\rho$) and atmospheric background extinction ($\Delta\alpha$) that are negligibly small. In that case, Eq. 4 reduces to

$$N_a = \frac{\ln(P_a/P_a')}{2(\sigma_a - \sigma_a')R} \quad (5)$$

The form given in Eq. 5, which greatly simplifies the relation between the lidar return ratio and species concentration, is frequently assumed in DIAL measurements, but Eq. 4 must be used in cases where either $\Delta\rho$ or $\Delta\alpha$ is nonnegligible. Equation 5 is valid for column-content or path-averaged DIAL measurements and is slightly changed for range-resolved measurements.

A large number of molecular species have been studied with the DIAL technique, and the results of many of these experiments are given in the proceedings of recent conferences (15), including extensive review articles on DIAL by T. Wilkerson and by E. Browell. The lidar systems used in these DIAL measurements span the frequency range from the UV to the IR and cover both range-

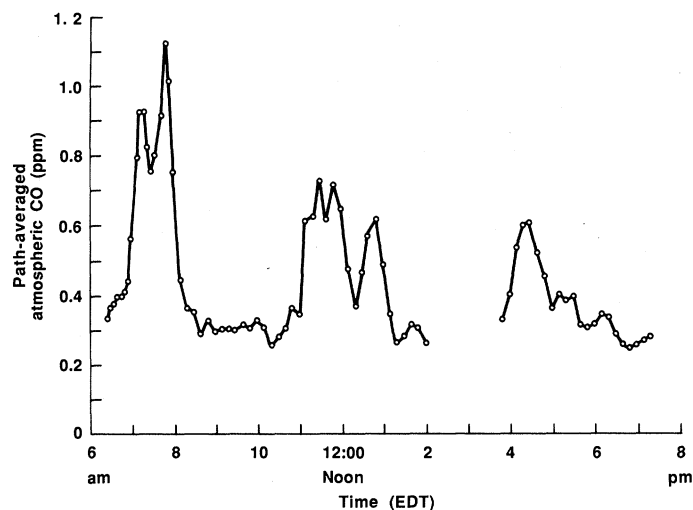


Fig. 6. CO₂ DIAL laser remote sensing of atmospheric CO for a path over a traffic roadway. Roadway range, 480 m; lidar range, 500 m.

resolved (RR) and path-averaged or column-content (CC) measurements.

Most DIAL experiments to date have used lidar signals backscattered from either a retroreflector or topographic targets (trees, buildings) to measure the column content of the atmospheric species between the laser transmitter and the target. Furthermore, most of these experiments have been carried out in the IR, where almost all molecules of interest have extensive absorption bands. The molecules investigated in CC DIAL experiments include SO₂, NH₃, O₃, CO, CO₂, HCl, H₂O, NO, N₂H₄, N₂O, and SF₆ (4-6, 21). The sensitivity of many of these CC DIAL measurements is on the order of a few parts per billion to a few parts per million, with detection ranges on the order of several kilometers. As an example, Fig. 6 shows time-averaged CC DIAL data obtained for the remote sensing of CO emitted by automobiles at a range of 500 m with a tunable CO₂ laser DIAL system (22). The increase in CO concentration during the morning, lunch, and evening rush hours is evident. The sensitivity of the DIAL measurement was approximately 10 ppb and the temporal resolution was approximately 1 second; the CO emission from individual vehicles was easily observed.

Range-resolved DIAL measurements provide a continuous signal as a function of range, based on the backscatter from atmospheric aerosols and particulates. As such, RR DIAL measurements have a significant advantage over CC DIAL measurements in that they can provide a three-dimensional map of the measured species. The major difficulty with RR DIAL is the relatively small backscatter coefficient for atmospheric aerosols and particulates compared to that for

Table 2. Selected list of atmospheric constituents and parameters measured by lidar. Accuracy and ranges given are typical values and depend upon individual lidar measurements.

Constituent or parameter	Laser type	Accuracy	Lidar type	Range (km)
Dust, clouds, volcanic ash, smoke plumes	Ruby, Nd:YAG	1 to 10%	Atmospheric backscatter	10 to 50
H ₂ O, O ₃ , SO ₂ , NO, NO ₂ , N ₂ O, C ₂ H ₄ , CH ₄ , HCl, CO, Hg, SF ₆ , NH ₃ , CO ₂	Dye, CO ₂ , OPO,* excimer, Co:MgF ₂	Variable, 1 ppb to 100 ppm	DIAL, Raman	1 to 5
OH, Na, K, Li, Ca, Ca ⁺	Dye	10 ² to 10 ⁷ atoms per cubic centimeter	Fluorescence	1 to 90
Temperature, pressure	Dye, Nd:YAG	1 K, 5 mbar	DIAL, Raman	1 to 30
Wind speed	CO ₂	0.5 m/sec	Doppler	15

*OPO, optical parametric oscillator.

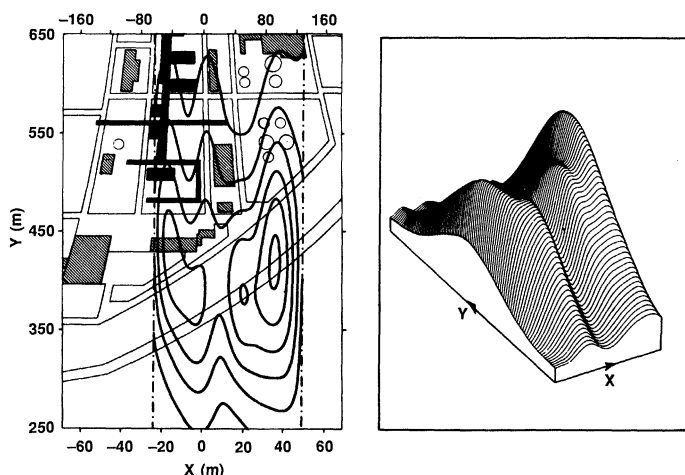


Fig. 7. Illustrations of the laser remote sensing of the concentration of ethylene near the distillation towers of a refinery. **(Left)** Isobars of concentration in increments of 20 ppb. **(Right)** Corresponding three-dimensional plot showing a peak concentration of approximately 150 ppb. [Adapted from (27)]

a hard target. Because of the small backscatter coefficients, most RR DIAL measurements have used relatively high-power lasers, or sophisticated optical detection techniques such as photon counting or heterodyne detection to increase sensitivity to the backscattered signal. In spite of these difficulties, several RR DIAL measurements of atmospheric molecules have been made. These measurements include the detection and mapping of SO_2 and NO_2 in a power plant plume (5), SO_2 and O_3 near urban centers (23), and NO_2 emitted by a chemical factory (24). Other examples are atmospheric temperature and pressure measurements based on absorption lines of oxygen near 760 nm (25) and precision measurements of O_3 in the upper atmosphere (26). These O_3 measurements are particularly important in light of the recent discovery of a “hole” in the atmospheric O_3 layer near Antarctica and the anticipated use of a similar DIAL system by NASA to study this phenomenon.

Finally, as an example of RR DIAL measurements, Fig. 7 shows data obtained by Rothe using a CO_2 laser DIAL system (27) which measured the concentration of ethylene (C_2H_4) over the area of a refinery. This figure illustrates the three-dimensional mapping capability of such a system.

Fluorescence lidar. In a fluorescence lidar system, the laser is tuned to an absorption line of the species that is to be measured and the reradiated fluorescence is detected by selective spectral filtering of the returned radiation. The fluorescence radiation may be at the same wavelength as the excitation wavelength or may be red-shifted (have a longer wavelength). In the latter case, a spectrometer or narrow-band interference filter is usually used to reject the strong Rayleigh backscatter and thus detect only the fluorescence signal. The backscatter coefficient for fluorescence is much greater in the UV than in the IR (Table 1); this is due to the combined effects of absorption cross section (greater in the UV than the IR) and radiative lifetime (longer in the IR than in the UV, which permits increased de-excitation due to collisions with ambient molecules).

Several factors that limit the application of fluorescence lidar for remote sensing include problems involving detector sensitivity coupled with solar background radiation, which generally reduces fluorescence measurements for remote sensing to nighttime investigations and to wavelengths shorter than 1 μm , where photomultiplier detection may be used. In addition, at tropospheric pressures an excited molecule will normally undergo several collisions with other molecules before fluorescent emission. This quenching of the excited molecule severely reduces the fluorescent output, rendering

it extremely inefficient for most remote sensing applications in the troposphere or even in the lower stratosphere.

In spite of these difficulties, several successful measurements of trace atmospheric species have been made with this technique. Ground-based visible fluorescence lidar systems have been developed by Megie (28) and by Gardner and his colleagues (29) and have been used to study alkali metal (sodium, potassium, lithium, calcium, Ca^+) concentration profiles at altitudes of 80 to 100 km (5, 28, 29). Peak sodium concentrations of about 10^3 to 10^4 atoms per cubic centimeter have been measured in the upper atmosphere; potassium concentrations, about an order of magnitude lower, and lithium atoms, with peak concentrations of approximately 1 atom per cubic centimeter at altitudes near 100 km, have been observed. The return signal from sodium atoms is sufficient to serve as a tracer to study temperature, eddy diffusion, and the dynamics of the wavelike features believed to be due to internal gravity waves and tidal effects in the upper atmosphere.

Another significant application of fluorescence lidar involves the study of the hydroxyl free radical, OH. Although OH occurs as a trace species at very low concentrations (on the order of 0.1 part per trillion), it plays an important catalytic role in various atmospheric chemistry processes and, together with chlorine and nitrogen oxides, is involved in the O_3 destruction cycle in the atmosphere. Airborne measurements of OH have been made with a laser operating at 282 nm (30). Concentrations on the order of 10^6 to 10^7 OH per cubic centimeter were observed, corresponding to approximately one part in 10^{13} . These measurements complement the extensive investigation of OH in the stratosphere in which a laser induced fluorescence spectrometer was mounted on a balloon-borne platform (31).

Raman scattering lidar. The use of Raman scattering methods for remote sensing is severely limited by the small optical interaction strength for Raman scattering. As a result, this technique is generally used with high-energy pulsed lasers, is restricted to the UV or visible regions of the spectrum so that sensitive photomultiplier tubes can be used for detection, and is most useful for the detection of species either at close range or in high concentration in the atmosphere such as N_2 , O_2 , and H_2O . It has a range capability of tens of kilometers for the detection of atmospheric N_2 but is limited to about a few hundred meters for pollution monitoring. In addition, its sensitivity is low (on the order of 100 ppm) as compared with other techniques. Despite these shortcomings, Raman scattering has several features that have made it a useful remote sensing tool. Its most noteworthy feature is that the laser wavelength does not have to be tuned across an absorption line since the spectral information is given by the frequency shift of the emission, which is independent of the laser wavelength. The strength of the scattering, except in certain resonance regions, is only weakly dependent on laser wavelength, and therefore Raman lidar does not require a particular laser frequency as long as the one chosen is effectively free of atmospheric interference.

The Raman-scattered wavelength-shifted spectra are distinct for each molecular species, which allows separate analysis of the Raman returns from each species. This spectral discrimination can be used to advantage by comparing the relative intensity of the returns from the molecule that is being detected to the intensity from atmospheric N_2 , whose concentration is known. This ratio approach simplifies a Raman lidar measurement by eliminating atmospheric or instrumental uncertainties in the lidar equation.

A wide variety of Raman lidar measurements of atmospheric polluting species have been made in regions where their concentrations are quite high. Reviews of such measurements are given by Inaba and Kobayashi (32), who discuss Raman lidar measurements of SO_2 , NO , CO , H_2S , C_2H_4 , CH_4 , and H_2CO present in high

concentration (100 to 1000 ppm) in oil smoke plumes and automobile exhausts, at ranges on the order of 30 to 100 m. Another application of Raman lidar arises from the fact that the backscattered Raman intensity for a given rotational band is strongly temperature dependent. This property has been used for the remote measurement of atmospheric temperature profiles at ranges of over 2 km with an uncertainty of less than ± 2 K. These results are described in a review by Cooney of the use of Raman scattering for the remote sensing of meteorological properties (33). In recent Raman lidar experiments, researchers have also studied water vapor profiles near the water-atmosphere boundary layer, subsurface ocean temperature profiles, and ocean turbidity. Long-range (30 km) measurements of atmospheric temperature by means of Raman lidar have also been reported (15, 34).

Doppler lidar. Doppler shifts in the return lidar signals have been used to measure wind velocities and to differentiate between molecular and aerosol returns in the atmosphere. Although these shifts are small (a fractional change in frequency of approximately 10^{-8} for a velocity of 1 m/sec at a wavelength of 10 μm), they can be measured by optical heterodyne detection techniques. Heterodyne detection involves the optical mixing of the lidar return with another laser operating at or near the lidar transmitter wavelength, with detection of the difference or beat frequency of the mixed signal.

Most Doppler lidar measurements have used 10- μm CO_2 lasers because CO_2 lasers offer high power and stable single-frequency operation (35–36). A review of work in this area, including a large bibliography, has been given by Bilbro (35). Recently, Hall and co-workers at NOAA used a CO_2 Doppler lidar to measure the velocity and direction of atmospheric wind fields at ranges up to 12 km (37). This system has yielded information on boundary layer flow near storm gust fronts and wind shears near airports; Fig. 8 shows a plot of wind speed and direction measured with Doppler lidar near Denver-Stapleton Airport during a storm, showing the presence of a wind shear–microburst (38). Doppler lidar systems have also been used to measure aircraft vortices and clear air turbulence. In particular, an airborne CO_2 laser system based at the NASA Marshall center has been used to construct two-dimensional vector wind fields in the vicinity of the aircraft in flight (39).

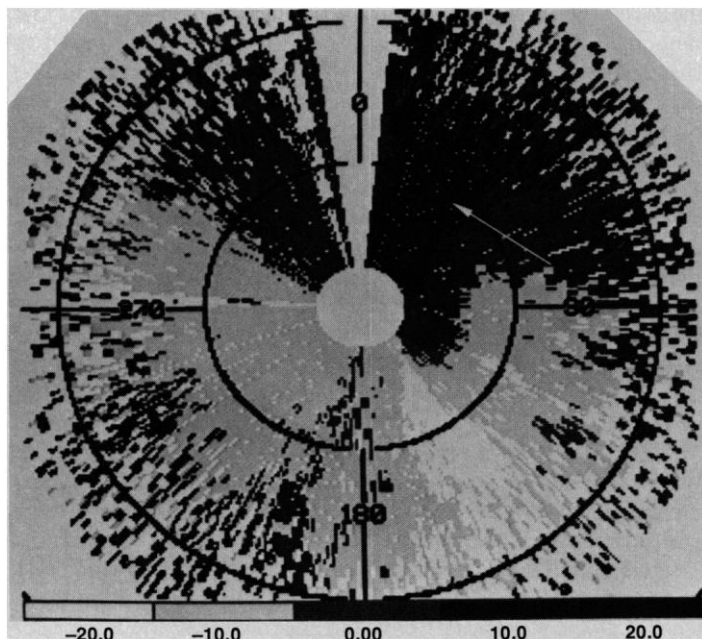


Fig. 8. Doppler lidar measurement of wind direction and velocity near Denver-Stapleton Airport during a storm; the arrow points to the presence of a strong, localized downburst-gustfront. [Adapted from (38)]

Doppler broadening effects have also been used by a University of Wisconsin group (40) to separate backscattered lidar signals into molecular and aerosol components. This distinction can be made because the Doppler broadening due to the thermal motion of molecules is about two orders of magnitude larger than that of the heavier aerosols. The separation is achieved by using a high-spectral-resolution Fabry-Perot optical interferometer to separate the Doppler-shifted molecular and nearly unshifted aerosol lidar returns. The system has been used in an aircraft to measure optical depth profiles and separate values of the molecular and aerosol backscatter cross sections as a function of height to an altitude of 1.6 km.

Accuracy Limitations

The accuracy of a lidar measurement is limited to the accuracy with which the average value of the lidar returns can be determined, and is therefore influenced by the statistical fluctuations of the lidar signals. These fluctuations are caused by several factors, including detector noise, changes in the propagation and attenuation characteristics due to atmospheric turbulence, changes in the geometry of the lidar beam and target, and variability in the laser power and wavelength. The limitations imposed by detector noise and signal fluctuations appear to be the dominant factors determining lidar measurement accuracy (20).

The noise level of the optical detector determines, in part, the accuracy or sensitivity of the lidar system; the lidar return signal must be greater than this noise level to be measured with precision. The ratio of the lidar signal strength and the noise of the system may be expressed analytically by noting that for a direct-detection lidar with a photodiode used for detection of the optical returns, the detector voltage signal-to-noise (S/N) ratio is given by (5, 41)

$$S/N = \frac{C P_r}{[D(P_r + P_B) + I_D + I_E]^{1/2}} \quad (6)$$

where P_B is the noise associated with the background radiation power incident on the detector, I_D is the dark current of the detector, I_E is the equivalent noise current of the detector preamplifier, and C and D are constants related to the signal bandwidth, optical wavelength, and detector quantum efficiency. A similar equation may be written for heterodyne detection, modified to include a local oscillator power term, and for optical detection with a photomultiplier tube or avalanche photodiode to include internal gain (6, 41). The denominator in Eq. 6 is associated with the shot noise of the system and is due to quantum fluctuations of the signal and noise currents. As expected, the S/N ratio for different types of lidar systems will depend on the noise characteristics of the optical detector and on the spectral filtering used in the system. It is often possible to choose a detector so that only one noise term in Eq. 6 is dominant; in this case, one can classify the detection process as being limited by the individual dominant noise source, such as signal shot noise, background noise, or amplifier noise. Optical detection in the UV, visible, and near IR (wavelengths up to 1 μm) uses photomultiplier tubes that have, under optimal conditions, exceptionally low noise levels, are capable of detecting a single photon of light, and are essentially shot noise–limited. Optical detection in the middle IR (1 to 10 μm) usually uses semiconductor materials for direct detection of the optical radiation; these devices are often background noise–limited and have noise levels that are several orders of magnitude higher than photomultiplier tube noise levels. Enhanced detection in the middle IR can be accomplished with optical heterodyne detection, which is capable of single photon detection, but only with a considerable increase in lidar complexity due to the addition of another laser used for optical mixing with the

lidar returns and, in the case of a DIAL system, the precision tunability and tracking of these laser wavelengths.

The accuracy of a lidar measurement is related to the lidar S/N ratio shown in Eq. 6 as $\sigma_0 = (S/N)^{-1}$, where σ_0 is the normalized statistical standard deviation of the fluctuating lidar returns and is a measure of the uncertainty in the estimate of the average value of the returns (41). It is well known that the accuracy of a measurement can be enhanced by signal averaging and that the S/N ratio or accuracy will increase as the square root of the number of pulses integrated. This may be expressed analytically as $\sigma_n = \sigma_0/n^{1/2}$, where σ_n is the standard deviation in the estimate of the mean value of the n pulses. This $n^{1/2}$ improvement in accuracy by signal averaging can be anticipated only if the measured returns from successive signals are uncorrelated, which means that the statistical properties of all the terms in Eq. 6 be temporally random (stochastic). In many lidar examples, the dominant noise sources are random and an $n^{1/2}$ improvement is observed. Such lidar measurements include, as examples, Raman and fluorescence lidar measurements of the upper atmosphere, DIAL measurements when atmospheric attenuation fluctuations are negligible, and the reduction of speckle (interference) effects in Doppler lidar measurements.

In some lidar measurements, however, the fluctuations observed are not random and are caused by long-term variability in the optical properties and attenuation of the atmosphere during the measurement period. This is often seen in DIAL measurements of the atmosphere, especially when the laser beam is transmitted in the lower atmosphere so that it is most susceptible to the influence of long-term drifts in the composition and temperature of the atmosphere near the surface of the earth. Under these conditions the statistical distribution and temporal characteristics of the terms in Eq. 6 are subject to both random and nonrandom influences, and a deviation from the expected $n^{1/2}$ improvement in the S/N ratio or σ_n is observed (42). An example of this effect is presented in Fig. 9, which shows a logarithmic plot of σ_n as a function of n , the number of lidar pulses averaged, for DIAL data obtained with a CO₂ laser; for comparison, a $n^{1/2}$ improvement is shown as the straight line in the figure. The marked deviation from $n^{1/2}$ behavior shown in Fig. 9 indicates the extent to which nonrandom processes may reduce the effectiveness of signal averaging. Figure 9 is only one example of this observed phenomenon; in fact, the deviation from $n^{1/2}$ behavior ranges from zero to values significantly greater than that shown. The physical sources of the correlation are believed to be atmospheric turbulence and long-term drifts, which lead to temporal changes in atmosphere attenuation during the measurement interval. Both of these effects would produce nonrandom fluctuations in the atmospheric attenuation, α , and thus influence the statistical properties of P_r .

In order to better understand the data shown in Fig. 9, we made a theoretical analysis to quantify the effect of correlation on a statistical ensemble of data, with direct application to DIAL (43). This analysis showed that the inclusion of correlation changes the simple $n^{-1/2}$ dependence of σ_n to

$$\sigma_n = \frac{\sigma_0}{n^{1/2}} \left[1 + 2 \sum_{j=1}^{n-1} (1 - j/n) \rho_j \right]^{1/2} \quad (7)$$

where ρ_j is the temporal autocorrelation coefficient for a delay time $j\tau$, and τ is the time interval between successive lidar measurements. For stochastic data, ρ_j is zero and Eq. 7 reduces to the $n^{-1/2}$ form as expected. As seen in Eq. 7, the effect of a nonzero value of ρ_j is to reduce the improvement in signal averaging. Further DIAL experiments (43) have shown that Eq. 7 is in excellent agreement with the observed DIAL data as presented in Fig. 9.

Equation 7 can be shown to reduce to $\sigma_n = \sigma_0 \rho_j^{1/2}$ for large n and

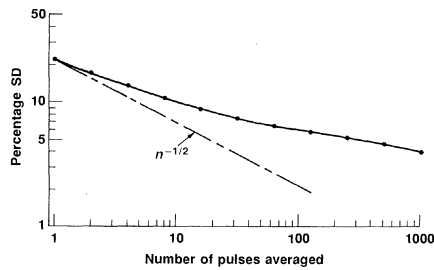


Fig. 9. Measurement accuracy (percent standard deviation) of CO₂ lidar signal returns from a diffusely reflecting target at a range of 2.7 km as a function of the number of pulses averaged. The reduced accuracy improvement relative to $n^{-1/2}$ behavior is due to long-term drifts in atmospheric attenuation.

nonzero ρ_j . This result shows that a limit exists, independent of n , for the improvement in the accuracy of a lidar measurement if nonrandom changes occur in the atmosphere during the measurement interval (43). Equation 7 is valid, in general, for all experimental measurements and describes quantitatively the often-observed diminished improvement from long-term averaging when nonrandom perturbations are causing changes in the average signal during the measurement period.

Finally, while Eq. 7 does predict the increase in accuracy of a lidar measurement through signal averaging, σ_n can be reduced by techniques that reduce either the initial values of σ_0 or the initial value of the correlation coefficient. These techniques (43–45) include the use of very high repetition rate lasers to increase the number of lidar samples collected before the atmosphere changes appreciably; the use of dual, nearly simultaneously transmitting, lasers for DIAL experiments; and the use of laser wavelength agility. Even with some of these techniques, the accuracy of most current lidar experiments has been limited to values on the order of a percent (that is, $\sigma_n \approx 1\%$) under optimal conditions and to values on the order of 1 to 10% under normal atmospheric conditions.

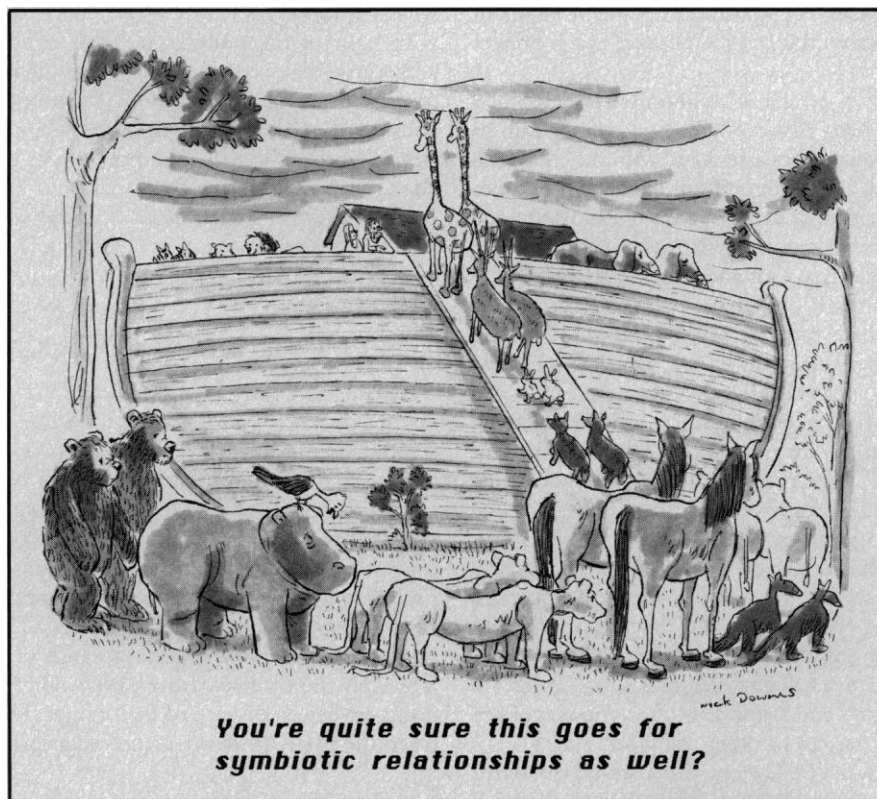
Future Directions

Laser remote sensing is a useful tool for probing the composition and physical state of the atmosphere and, by means of single-ended measurements at a distance, permits measurements at locations that cannot be reached with conventional detection methods such as chemical or optical point sensors. Although technical limitations do exist, in many instances, lidar offers the only realistic measurement technique that can detect a physical quantity and produce a three-dimensional map of the quantity in real time.

The future of laser remote sensing appears to be quite promising and is dependent upon factors that include (i) the development of practical, new, eye-safe laser sources that cover the spectral gaps shown in Fig. 4, (ii) further reduction of lidar system complexity, cost, and size, and (iii) the future use of lidar techniques in new applications. Among the latter are several emerging industrial and medical applications that include the use of fiber optics in enclosed or hostile environments, the use of airborne lidars for oil, gas, and geological exploration, and the exploitation of the long-range (>100 km) detection capability and wide surveillance potential of space-borne laser remote sensing. Examples that are currently being explored include (i) the detection of methane gas leaks in a coal mine with a diode laser lidar system, (ii) the use of a laser coupled to a low-loss optical fiber network to detect methane or natural gas leaks in an industrial processing plant, (iii) the Doppler lidar measurement of global wind fields from a satellite to increase the accuracy of weather forecasts, and (iv) the planned use of lidar aboard the NASA space-borne Earth Observing System for global temperature, water vapor, and pressure measurements.

REFERENCES AND NOTES

1. A. I. Carswell, *Can. J. Phys.* **61**, 378 (1983).
2. H. Kildal and R. Byer, *Proc. IEEE* **59**, 1644 (1971).
3. R. Byer, *Opt. Quantum Electron.* **7**, 147 (1975).
4. E. D. Hinkley, Ed., *Laser Monitoring of the Atmosphere* (Springer-Verlag, Berlin, 1976).
5. D. K. Killinger and A. Mooradian, Eds., *Optical and Laser Remote Sensing* (Springer-Verlag, Berlin, 1983).
6. R. M. Measures, *Laser Remote Sensing: Fundamentals and Applications* (Wiley, New York, 1984).
7. L. D. Smullin and G. Fiocco, *Nature (London)* **194**, 1267 (1962); G. Fiocco and L. D. Smullin, *ibid.* **199**, 1275 (1963).
8. M. G. H. Ligda, in *Proceedings of the 1st Conference on Laser Technology*, U.S. Navy ONR (1963), pp. 63-72.
9. R. M. Schotland, in *Proceedings of the 4th Symposium on Remote Sensing of the Environment*, 12 to 14 April 1966, University of Michigan, Ann Arbor, p. 273.
10. E. D. Hinkley and P. L. Kelley, *Science* **171**, 635 (1971).
11. W. Driscoll and W. Vaughan, Eds., *Handbook of Optics* (McGraw-Hill, New York, 1978); H. W. Yates and J. H. Taylor, *Infrared Transmission of the Atmosphere* (Report 5453 AD 240188, U.S. Naval Research Laboratory, Washington, DC, 1960).
12. The values for ρ shown in Table 1 for atmospheric species were derived with a range resolution, ΔR , of 100 m and the simplifying assumption of isotropic scattering. For the case of Rayleigh, Mie, and Raman scattering, the effective reflectivity, ρ , is related to the volume backscatter coefficient and thus to the extinction coefficient, α , for each individual interaction. For the case of absorption, as noted in the text, the value of ρ corresponds to backward-directed fluorescence emission of the atom or molecule after it has absorbed the incident light. For atmospheric species, this fluorescence process is efficient in the UV and visible part of the spectrum but suffers considerably in the IR because of collisional quenching with other atmospheric molecules during the long lifetime of an IR transition.
13. *Laser Focus Buyers Guide* (Penn Well, Tulsa, OK, 1986), pp. 47-133.
14. *Tunable Solid State Lasers—Technical Digest* (topical meeting, Optical Society of America, 16 and 17 May 1985, Washington, DC) (Optical Society of America, Washington, DC, 1985).
15. *Eleventh International Laser Radar Conference* (Conference Publication 2228, NASA, Washington, DC, 1982); *Twelfth International Laser Radar Conference Proceedings* (Aix-en-Provence, 1984); *Optical Remote Sensing of the Atmosphere—Technical Digest* (Optical Society of America, Washington, DC, 1985); *Optical Techniques for Remote Probing of the Atmosphere—Technical Digest* (Optical Society of America, Washington, DC, 1983). Several papers based on submissions at these conferences have been published in *Appl. Opt.* **22**, 2527 (1983); *ibid.*, p. 3684; *ibid.* **24**, 3443 (1985).
16. M. P. McCormick, *Opt. Eng.* **21**, 340 (1982); ——— and T. J. Swisler, *Geophys. Res. Lett.* **10**, 877 (1983).
17. E. E. Uthe et al., *Bull. Am. Meteorol. Soc.* **61**, 1035 (1980).
18. P. Chýlek, G. W. Grams, R. G. Pinnick, *Science* **193**, 480 (1976); J. Heintzenberg, J. H. Muller, H. Quenzel, E. Thomalla, *Appl. Opt.* **20**, 1308 (1981).
19. G. W. Kattawar and G. N. Plass, *Appl. Opt.* **15**, 3166 (1976).
20. N. Menyuk and D. K. Killinger, *ibid.* **22**, 2690 (1983).
21. W. B. Grant and R. T. Menzies, *J. Air Pollut. Control Assoc.* **33**, 187 (1983).
22. D. K. Killinger, N. Menyuk, W. E. DeFeo, *Appl. Phys. Lett.* **36**, 402 (1980).
23. E. V. Browell, *Opt. Eng.* **21**, 128 (1982).
24. K. W. Rothe, U. Brinkman, H. Walther, *Appl. Phys.* **4**, 181 (1974).
25. C. L. Korb and C. Y. Weng, *Appl. Opt.* **22**, 3759 (1983).
26. J. Werner, K. W. Rothe, H. Walther, *Appl. Phys. B* **32**, 113 (1983); O. Uchino, M. Tokunaga, M. Macda, Y. Miyozoe, *Opt. Lett.* **8**, 347 (1983).
27. K. W. Rothe, *Radio Electron. Eng.* **50**, 567 (1980).
28. G. Megie, F. Bos, J. E. Blamont, M. L. Chanin, *Planet. Space Sci.* **26**, 27 (1978).
29. J. R. Rowlett, C. S. Gardner, E. S. Richter, C. F. Sechrist, *Geophys. Res. Lett.* **5**, 683 (1978).
30. C. C. Wang, L. I. Davis, Jr., P. M. Selzer, *J. Geophys. Res.* **86**, 1181 (1981); D. D. Davis, W. Heaps, T. McGee, *Geophys. Res. Lett.* **3**, 331 (1976).
31. J. G. Anderson, *Geophys. Res. Lett.* **3**, 165 (1976); W. S. Heaps, *Appl. Opt.* **19**, 243 (1980); ——— and T. J. McGee, *J. Geophys. Res.* **90**, 7913 (1985).
32. H. Inaba and T. Kobayashi, *Opto-electronics* **4**, 101 (1972); H. Inaba, in (4), chap. 5.
33. J. A. Cooney, *Opt. Eng.* **22**, 292 (1983).
34. S. H. Melfi and D. Whiteman, *Bull. Am. Meteorol. Soc.* **66**, 1288 (1985); D. A. Leonard, *Opt. Eng.* **20**, 91 (1981); F. E. Hoge and R. N. Swift, *Appl. Opt.* **22**, 3778 (1983); S. H. Melfi and D. Whiteman, in *Proceedings of the 13th International Laser Radar Conference* (Conference Publication 2431, NASA, Washington, DC, 1986), p. 188.
35. J. W. Bilbro, *Opt. Eng.* **19**, 533 (1980).
36. R. Teoste and R. N. Capes, *J. Appl. Meteorol.* **17**, 1575 (1978).
37. F. F. Hall, Jr., et al., *Appl. Opt.* **23**, 2503 (1984).
38. R. M. Hardesty, K. Elmore, M. E. Jackson, in *21st Conference on Radar Meteorology* (American Meteorological Society, Boston, 1983).
39. J. Bilbro, G. Fichtl, D. Fitzjarrald, M. Krause, R. Lee, *Bull. Am. Meteorol. Soc.* **65**, 348 (1984).
40. S. T. Shipley et al., *Appl. Opt.* **22**, 3716 (1983); *ibid.*, p. 3725.
41. This equation refers to the definition for S/N ratio used in communication theory. A more general definition of lidar S/N includes the concept of carrier-to-noise ratio and the effects of target speckle and atmospheric turbulence. See, for example, J. H. Shapiro, B. A. Capron, R. C. Harney, *Appl. Opt.* **20**, 3292 (1981).
42. D. K. Killinger and N. Menyuk, *IEEE J. Quantum Electron.* **QE-17**, 1917 (1981); ———, W. E. DeFeo, *Appl. Opt.* **22**, 682 (1983).
43. N. Menyuk, D. K. Killinger, C. R. Menyuk, *Appl. Opt.* **21**, 3377 (1982); *ibid.* **24**, 118 (1985).
44. B. J. Rye, *J. Appl. Meteorol.* **22**, 1899 (1983).
45. R. C. Harney, *Appl. Opt.* **22**, 3747 (1983).
46. This work was supported by the National Aeronautics and Space Administration and the Air Force Engineering and Services Center.



You're quite sure this goes for symbiotic relationships as well?